European Journal of Medicinal Chemistry 123 (2016) 354–364

Contents lists available at ScienceDirect

European Journal of Medicinal Chemistry

journal homepage: http://www.elsevier.com/locate/ejmech

Research paper

α–*N*–heterocyclic thiosemicarbazone Fe(III) complex: Characterization of its antitumor activity and identification of anticancer mechanism

Yi Gou, Jun Wang, Shifang Chen, Zhan Zhang, Yao Zhang, Wei Zhang, Feng Yang*

School of Pharmacy, Nantong University, Nantong, Jiangsu, China

ARTICLE INFO

Article history:
Received 17 August 2015
Received in revised form
12 July 2016
Accepted 19 July 2016
Available online 26 July 2016

Keywords:
Iron(III) complex
α–*N*–heterocyclic thiosemicarbazone
DNA cleavage
Anticancer activity
Anticancer mechanism

ABSTRACT

We synthesized an α–*N*–heterocyclic thiosemicarbazone ligand (L) and its Fe complex (**C1**) and assessed their chemical and biological properties in order to understand their marked activity. Electrochemical studies and ascorbate oxidation studies demonstrated that **C1** shows considerable redox activity, and $Fe^{III/II}$ redox potentials was within the range accessible to cellular oxidants and reductants. Absorption spectral, emission spectral and viscosity analysis reveal that L and **C1** interacted with DNA through intercalation and **C1** exhibited a higher DNA binding ability. Agarose gel electrophoresis experiments indicated that **C1** exhibited the highest pBR322 DNA cleaving ability. *In vitro*, **C1** showed significantly more anticancer activity than the ligand alone. Moreover, **C1** induces production of reactive oxygen species (ROS) and DNA damage, resulting in activation of the p53 pathway, cell cycle arrest at the S phase, and mitochondria-mediated apoptosis by regulating the expression of Bcl–2 family proteins.

1. Introduction

Metal coordination complexes offer biological and chemical diversity that is distinct from that of organic drugs [1–3]. For decades, *cis*platin and its derivatives are used in more than 50% of the treatment regimes for patients suffering from cancer [4,5]. However, the toxicities coupled with acquired and intrinsic drug resistance, have hampered theirs broad clinical application [6–8]. These unresolved disadvantages stimulate research on most desirably with reduced side effects, more efficacious, a broader spectrum of indication and higher selectivity metal–based anticancer compounds.

Iron (Fe) is an essential trace element in biological systems and catalyzes key reactions involved in metabolism, oxygen transport, respiration, and DNA synthesis [9]. Many studies have shown that rapidly growing tumor cells, such as leukemia and neuroblastoma, have particularly high demands for Fe [10,11]. It is believed that the antitumor activity of Fe is two–fold: (1) neoplastic cells generally proliferate at a faster rate than their normal counterparts and express higher levels of the transferrin receptor 1, which is necessary for Fe cellular uptake of from serum Fe-transport protein, transferrin, at a rapid rate [12–14]; and (2) cancer cells express higher levels of the Fe-containing enzyme such as the ribonucleotide reductase [15], being a catalyst of the rate-limiting step of DNA synthesis [16]. These characteristics suggest that iron represents a potential therapeutic target for cancer treatment.

On the other hand, thiosemicarbazones are an emerging class of ligands that show pronounced and selective antitumor activity and can overcome resistance to standard chemotherapy [17–23]. Especially α–*N*–heterocyclic thiosemicarbazones with a nitrogen containing heterocycle in a position to the thiosemicarbazide side chain exert significant antitumor activity *in vitro* and *in vivo* [24,25]. For instance, Triapine (3-aminopyridine-2-carboxaldehyde thiosemicarbazone) has been tested in a variety of tumor cell lines in the preclinical setting and is currently undergoing different phase I and II clinical trials [26]. A recent study of a phase II trial of triapine (105 mg/m^2/day) demonstrated that the overall response rate was 49%, with a complete remission rate of 24% [27]. Interestingly, the biological activities of thiosemicarbazone can be modified by the linkage to important metal ions such as Fe, Ni, Cu and Zn [28–30]. Thus, development of thiosemicarbazones compounds that chelate Fe has become a therapeutic strategy showing significant promise. However, previous studies have illustrated that complexation of some thiosemicarbazones ligands such as Bp44 mT, Dp44 mT, NBp4mT, HDp4pT and NBpT ligands with Fe can result in

* Corresponding author. 9 Seyuan Road, Nantong, Jiangsu, 226019, China.
E-mail address: fyang@mailbox.gxnu.edu.cn (F. Yang).

http://dx.doi.org/10.1016/j.ejmech.2016.07.041
0223-5234/

significantly decreased antiproliferative activity when compared to the free ligands [20,31,32]. In contrast, similar thiosemicarbazones ligands such as BpT and HDp4mT showing less activity than their Fe complexes are often noticed [31,32]. Therefore, the mechanisms involved in the antitumor activities of thiosemicarbazones Fe complexes are far from clear.

In an effort to discover novel thiosemicarbazones derivatives with potent anticancer activity and to elucidate their mechanism of action, thiosemicarbazone bearing condensed α–*N*–heterocyclic moiety ligand (L) and its Fe complex ($[Fe(L)_2]NO_3$) were synthesized. We not only comprehensively characterized their chemical and biological properties but also determined Fe complex mechanism of action for HepG2 cells *in vitro*. Thus, our results are important for further understanding the pronounced biological activity of these complexes.

2. Experimental section

All solvents and chemicals used were of high purity and available from commercial sources. Water used in the reactions was distilled prior to use. Elemental analyses (C, N and H) were performed on a Perkin–Elmer 2400 analyser. Infrared (IR) spectra of all samples were recorded using KBr pellets on a Nexus 870 FT–IR spectrophotometer in the frequency of 400–4000 cm^{-1}. UV–visible spectra were measured in DMSO-buffer solution on a Cary 1E UV–Visible spectrophotometer in the 200–800 nm range.

2.1. Synthesis and structures of L ligand and Fe(III) complex

2.1.1. Synthesis of L ligand and Fe(III) complex

Synthesis of L. A solution of *N*-phenylhydrazinecarbothioamide (1.67 g, 10 mmol) in MeOH (15 mL) was added to a methanolic solution (15 mL) of quinoline-2-carbaldehyde (1.57 g, 10 mmol) and the mixture refluxed for 1 h. The mixture was kept in air for a week, forming yellow block crystals. Yield: 71%. *Anal.* Calcd for $C_{17}H_{14}N_4OS$ (322.38): C, 63.33; H, 4.38 and N, 17.38. Found: C, 62.95; H, 4.67 and N, 17.27. IR (KBr, cm^{-1}): 3651w, 3126s, 2977 m, 1594vs, 1535vs, 1443 m, 1398 m, 1344s, 1311 m, 1186s, 1099 m, 1026s, 932 m, 895 m, 827s, 788w, 690s, 621 m, 460 m. ^1H NMR ([D_6]DMSO): δ = 12.20 (s, 1H), 10.39 (s, 1H), 8.62 (d, *J* = 8.7 Hz, 1H), 8.43–8.33 (m, 2H), 8.02 (dd, *J* = 17.0, 8.2 Hz, 2H), 7.78 (t, *J* = 7.6 Hz, 1H), 7.67–7.53 (m, 3H), 7.41 (t, *J* = 7.8 Hz, 2H) and 7.25 (t, *J* = 7.3 Hz, 1H). ^{13}C NMR ([D_6]DMSO): δ = 177.06, 154.25, 147.85, 143.56, 139.44, 136.69, 130.41, 129.29, 128.61, 128.39, 128.38, 127.69, 126.78, 126.13 and 118.91 ppm.

*Synthesis of $[Fe(L)_2]NO_3$ (**C1**).* The L ligand (2 mmol) was dissolved in MeOH (15 mL). Then 0.482 g of $Fe(NO_3)_3$ was added to the basic ligand solution, and the mixture was gently refluxed for 30 min at room temperature to give a celadon solution and then filtered. The filtrate was kept in air for a week, forming blank block crystals. The crystals were isolated, washed three times with distilled water and dried in a vacuum desiccator containing anhydrous $CaCl_2$. Yield: 63%. *Anal.* Calcd for $C_{34}H_{26}FeN_9O_3S_2$ (728.61): C, 56.04; H, 3.49 and N, 17.30. Found: C, 55.31; H, 3.53 and N, 17.17. IR (KBr, cm^{-1}): 3647w, 2974 m, 1596vs, 1540vs, 1502s, 1471s, 1424s, 1317s, 1185s, 1107s, 993 m, 936 m, 878 m, 825 m, 748s, 689 m, 619 m, 532w, 497 m.

2.1.2. Crystal structures determination of Fe(III) complex

Single crystal X–ray crystallographic data were collected on a Bruker SMART Apex II CCD diffractometer at room temperature using graphite-monochromated Mo–Kα (λ = 0.71073 Å) radiation. Empirical adsorption corrections were applied to all data using SADABS program. The structures were solved by direct methods and refined with by full–matrix least–squares methods on F^2 using the SHELXTL version 5.1 [33]. All of the non–hydrogen atoms were refined anisotropically. All hydrogen atoms were placed in geometrically ideal positions and constrained to ride on their parent atoms. The crystallographic data for complexes L and **C1** are summarized in Table 1, and selected angles and bond lengths are given in Table 2. Crystallographic data for the structural analyses have been deposited at the Cambridge Crystallographic Data Centre, reference numbers 1418471 for L and 1418470 for **C1**. The crystallographic data can be obtained free of charge from the Cambridge Crystallographic Data Centre via http://www.ccdc.cam.ac.uk/data_request/cif.

2.1.3. Density functional theory (DFT) calculations

All of the calculations were done with the GAMESS suite of codes [34] and the atomic coordinates were obtained from the X–ray structures (Table S1). Full geometry optimization of all structures was carried out at the density functional theory (DFT) level of theory using B3LYP method [35,36]. Symmetry operations were not applied for all structures. Geometries and the reported Gibbs energies were optimized employing the 6–31 + G(d,p) basis set for all atoms. Solvation effects were taken into account using the integral equation formalism (IEF–PCM) [37] model.

2.2. Cyclic voltammetry

Cyclic voltammetry was carried out with a BAS100B/W potentiostat. The electrochemical measurements were performed in a conventional two compartment three electrode cell with a glassy carbon as a working electrode, an aqueous Ag–AgCl as a reference electrode (E^o = 196 mV *vs* NHE), and platinum (Pt) wire as a counter electrode. To ensure the solubility of this complex, the complex **C1** was at 1 mM in MeCN/H_2O (70:30 v/v). The supporting electrolyte was Et_4NClO_4 (0.1 M), and the solutions were purged with nitrogen prior to measurement.

2.3. Ascorbate oxidation assay

Ascorbate oxidation assay were investigated as described in an earlier report [38]. Briefly, ascorbic acid (100 μM) was prepared immediately prior to an experiment and incubated in the presence of $Fe(NO_3)_3$ (10 μM), the L ligand (ligand:Fe(III) ratios = 0.1, 1, or 3) and a 50–fold molar excess of citrate (500 μM). The absorbance at 265 nm was recorded after 10 and 40 min at room temperature, and the decrease of intensity between these time points was calculated [39].

Table 1
Crystal data for complexes HL and **C1**.

Complex	HL	C1
Empirical formula	$C_{17}H_{14}N_4OS$	$C_{34}H_{26}FeN_9O_3S_2$
Molecular weight	322.38	728.61
Crystal system	monoclinic	orthorhombic
Space group	$P2_1/c$	*Pbca*
a (Å)	10.519(5)	16.3360(4)
b (Å)	7.173(3)	18.0196(4)
c (Å)	22.858(12)	21.4266(5)
α (°)	90.00	90.00
β (°)	98.85(5)	90.00
γ (°)	90.00	90.00
T (K)	296.15	293.15
V (Å^3)	1704.0(14)	6307.3(2)
Z	4	8
$\rho_{calc.}$ ($g \cdot cm^{-3}$)	1.257	1.535
F(000)	672	3000
μ(Mo-K$_\alpha$) (mm^{-1})	0.199	0.664
Data/restraint/parameters	2991/0/217	6455/0/442
Goodness-of-fit on F^2	1.002	1.038
Final R_1, wR_2 [$I > 2\sigma(I)$]	0.0957, 0.2164	0.0513, 0.0970

Table 2
Selected bond lengths [Å] and angles [°] in complexes HL and **C1**.

HL			
S1–C7	1.672(7)	N2–C7–S1	118.0(5)
N2–C7	1.351(8)	N1–C7–S1	126.8(6)
N2–N3	1.379(7)	C7–N2–N3	120.6(6)
N4–C9	1.312(7)	N1–C –N2	115.2(6)
N4–C17	1.352(8)	C8–N3–N2	116.8(6)
C1			
Fe1– S2	2.2109(9)	N5–Fe1–N1	91.19(10)
Fe1–N5	2.056(2)	N5–Fe1–S1	87.18(7)
Fe1–N2	1.918(3)	N2–Fe1–S2	88.33(8)
Fe1–N1	2.062(2)	N2–Fe1–N5	107.60(10)
Fe1–N6	1.912(3)	N2–Fe1–N1	80.99(10)
Fe1–S1	2.2170(9)	N2–Fe1–S1	83.61(8)
S2–Fe1–S1	97.19(4)	N1–Fe1–S2	88.96(7)
N5–Fe1–S2	163.89(8)	N1–Fe1–S1	163.24(8)
N6–Fe1–S2	83.97(8)	N6–Fe1–N2	169.39(11)
N6–Fe1–N5	80.51(10)	N6–Fe1–N1	106.08(10)
N6–Fe1–S1	90.11(8)		

2.4. DNA binding experiments

2.4.1. UV spectroscopy

Electronic absorption spectra were determined in the range of 240–650 nm by gradually increasing the amounts of calf-thymus DNA (CT-DNA) to the complexes (20 μM) in 5 mM Tris-HCl–50 mM NaCl buffer. Then, the resulting solutions were allowed to equilibrate at room temperature for 5 min. In order to affirm quantitatively the affinity of the complexes L and **C1** bound to DNA, the binding constant (K_b) was obtained by using the following equation [40].

$$[DNA]/(\varepsilon_a-\varepsilon_f) = [DNA]/(\varepsilon_b-\varepsilon_f) + 1/K_b(\varepsilon_b-\varepsilon_f) \quad (1)$$

where [DNA] is the concentration of DNA in base pairs and the apparent molar extinction coefficients ε_a, ε_b and ε_f correspond to A_{obs}/[complex], the extinction coefficient of free (unbound) and the fully bound complexes, respectively.

2.4.2. Fluorescence spectroscopy

The competitive binding study was carried out by maintaining the ethidium bromide (EB, 2.5 μM) and CT-DNA (4 μM) in Tris-HCl buffer (pH 7.2), and increasing the concentrations of the complexes L and **C1**. The fluorescence spectra were recorded between 550 and 800 nm at room temperature with the excitation wavelength set at 530 nm. The complexes L and **C1** did not emit fluorescence at the excitation and emission wavelengths. For every addition, the sample was shaken and allowed to stand for 5 min, and then the fluorescence emission spectra were recorded. Further, the apparent binding constant (K_{app}) has been calculated from equation (2) [41].

$$K_{EtBr}\,[EB] = K_{app}\,[complex] \quad (2)$$

where [EB] = 2.5 μM and K_{EtBr} is 1×10^7 M^{-1}; [complex] is the concentration of the complex causing 50% reduction in the emission intensity of EB.

2.4.3. Viscosity experiments

The relative change in viscosity was measured using an Ubbelodhe viscometer, immersed in a thermostated water-bath maintained at 30 ± 0.5 °C. The concentration of DNA was 200 μM and increasing concentrations of complexes were used. Each complex solution was measured three times and an average flow time was calculated. Data are presented as $(\eta/\eta_o)^{1/3}$ versus the ratio of the concentration of the complexes to CT-DNA, where η_o is the viscosity of CT-DNA alone and η is the viscosity of CT-DNA in the presence of the complex.

2.5. DNA cleavage experiment

The cleavage of DNA was studied by agarose gel electrophoresis. Reactions using supercoiled pBR322 plasmid DNA in 1 × TBE (Tris–borate–EDTA) buffer (pH 7.26) was treated with the complexes L and **C1** (5–15 μM) by dilution with the 1 × TBE buffer to a total volume of 20 μL. The mixture was then incubated for 3 h at 37 °C, and then the loading buffer was added. The resulting solutions were electrophoresed for 50 min at 100 V on 1% agarose gels containing 5 μL goldview in 1 × TBE buffer. Then, the gel bands were visualized and photographed on a BIO-RAD Laboratories Segrate gel imaging system.

2.6. Cell lines

The human breast cancer cell lines MCF-7, drug-resistant MCF-7/ADR cells, human cervical cancer cell lines HeLa, human liver hepatocellular carcinoma cell lines HepG2 and human liver cell lines HL-7702 (purchased from the American Type Culture Collection and the German Collection of Microorganisms and Cell Cultures) were maintained in DMEM or RPMI-1640 supplemented with 10% fetal bovine serum (FBS), 50 U/mL penicillin, 50 mg/mL streptomycin at 37 °C and 5% CO_2.

2.7. 3–(4,5–Dimethylthiazol–2–yl)–2,5–diphenyltetrazolium bromide (MTT) assays

All compounds were dissolved in PBS with 0.5% DMSO and then tested. The 100 μL of cell suspensions at a density of 5×10^4 cells/mL was seeded in triplicate in 96–well plates and incubated for 24 h at 37 °C in 5% carbon dioxide atmosphere. Then the medium was removed and replaced with the respective medium with 10% FBS containing the compounds at the appropriate concentrations and incubated at 37 °C under conditions of 5% CO_2 for 48 h. 10 μL MTT dye (5 mg/mL) was added to each well. After incubation for another 4 h, the absorbance was read by enzyme labeling instrument with 570/630 nm double wavelength measurement. The cytotoxicity was evaluated based on the percentage of cell survival compared with the negative control. The final IC_{50} values were calculated by the Bliss method (n = 5). All the tests were repeated in at least three independent experiments.

2.8. Anticancer mechanism of Fe(III) complex

2.8.1. Apoptosis by flow cytometry

The apoptotic events induced by **C1** were determined by annexin V staining and PI staining according to the manufacturer's protocol for the Annexin V–FITC Apoptosis Detection Kit (Abcam). Briefly, HepG2 cells were seeded in 6-well plates at 2.0×10^5 cells/well in 2 mL of complete DMEM and cultured for 24 h. The cells were incubated at 5% CO_2 and 37 °C with the **C1** at indicated concentrations. The HepG2 cells without the treatment were used as a control. After 24 h, cells were harvested and resuspended in 200 μL 1 × annexin V–binding buffer. Next, 5 μL each of annexin V and PI were added to each sample and incubated on ice for 15 min. The samples were analyzed by flow cytometry (FACScan, Bection Dickinson, San Jose, CA). The rate of cell apoptosis was analyzed.

2.8.2. Acridine orange/ethidium bromide (AO/EB) double staining

HepG2 cells were treated with **C1** (0.2 μM and 0.4 μM) at a fixed incubation time of 24 h, respectively. After incubation, cells were washed twice with PBS and fixed with 4% paraformaldehyde. Then,

the cells were stained with AO/EB staining solution for 5 min. After washing twice with PBS, the cells of morphological observation were obtained under a reflected fluorescence microscope (Nikon MF30 LED, Japan).

2.8.3. Cell cycle distribution analysis

Cell cycle distribution was analyzed by PI staining and flow cytometry. HepG2 cells were exposed to **C1** at the indicated concentrations. After 24 h incubation, the cells were collected, washed for twice with ice-cold PBS, fixed with 70% ethanol at 4 °C overnight and treated with Rnase A for 35 min at 37 °C, followed by PI staining for 15 min in the dark. Percentage of cells in different cell cycle phases was measured by flow cytometry using a 488 nm laser (FACScan, Bection Dickinson, San Jose, CA).

2.8.4. Intracellular reactive oxygen species (ROS) measurements

Intracellular ROS generation was determined using 2′,7′–dichlorodihydro–fluorescein diacetate (H_2DCF–DA) (Beyotime Institute of Biotechnology, Haimen, China). Briefly, 2 mL HepG2 cells (2×10^5 cells per well) were seeded in 6-well plates and cultured for 24 h. Then cells were incubated with **C1** at indicated concentrations for 24 h at 37 °C. Cells were collected for flow cytometric assessment. The fluorescence intensity was monitored with excitation wavelength at 488 nm and emission wavelength at 525 nm.

2.8.5. The change of mitochondrial membrane potential assay

Mitochondrial membrane potential was measured by a fluorescent dye JC–1 (Beyotime, Haimen, China). HepG2 cells were treated with different concentrations **C1** in 6–well plates and PBS was used as a control. Cells were harvested and washed twice with PBS after 24 h of incubation. Subsequently, cells were stained with 1 mL of JC–1 stock solution (10 μg/mL). Assays were initiated by incubating HepG2 cells with JC–1 for 30 min at 37 °C in the dark and the fluorescence of separated cells was detected with a flow cytometer (FACScan, Bection Dickinson, San Jose, CA).

2.8.6. Western blot analysis

HepG2 cells were seeded into 3.5 cm dishes for 24 h, and then exposed to **C1** at indicated concentrations for 24 h at 37 °C. Cells were harvested and washed with ice–cold PBS three, then were lysed in radioimmunoprecipitation assay (RIPA) buffer. The protein concentration of the supernatant was determined by BCA (bicinchoninic acid) assay. Equal amounts of cellular total proteins were separated on 10% SDS–polyacrylamide gel electrophoresis and then transferred onto poly(vinylidene difluoride) (PVDF) membranes (Millipore, MA, USA). The PVDF membranes were blocked with 5% (w/v) non–fat milk in TBST buffer (20 mM Tris, pH 8.0, 150 mM NaCl, and 0.05% Tween 20) for 1 h. Then, the membranes were incubated with the primary antibodies (Cell Signalling Technology and Santa Cruz) overnight at 4 °C. After a subsequent washing step, the membrane is incubated with the appropriate secondary antibodies conjugated with horseradish peroxidase (Cell Signalling Technology) for 1 h at room temperature and washed for three times with TBST. The immunoreactivity was detected using Amersham ECL Plus (Amersham) western blotting detection reagents.

2.9. Statistical analysis

All biological experiments were repeated 3 to 5 times. Student's *t*-test was applied to evaluate the significance of differences measured. The representative results were expressed as mean ±standard deviations (SD) and considered to be significant when $p < 0.05$.

3. Results and discussion

3.1. L ligand and Fe(III) complex characterization

The structure of L was solved in the space group $P2_1/c$ and monoclinic molecule with one independent molecule in a unit cell. Fig. 1A shows the molecular structure of L, which is intersectant with the dihedral angle between the phenyl ring and pyridine ring of 49.4°. The monomeric units of L are arranged in a dimer fashion

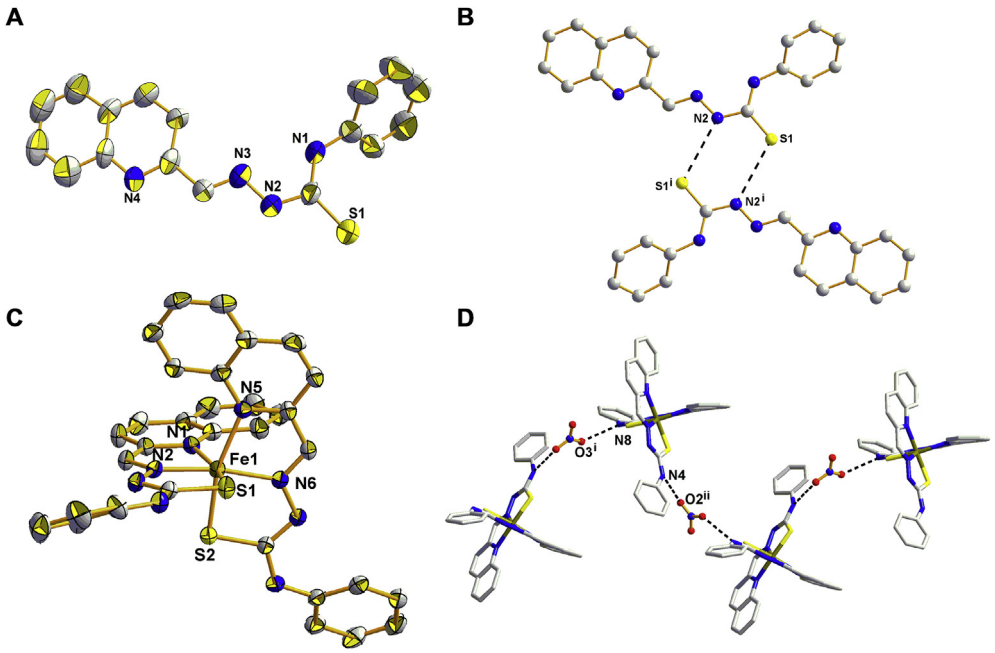

Fig. 1. (A) Ortep drawings of L with 50% probability displacement ellipsoids. Hydrogen atoms and H_2O are omitted for clarity. (B) The N–H···S interactions in L (Symmetry code: i = 1 − *x*, 2 − *y*, − *z*). (C) The local coordination environment of C**1**. Displacement ellipsoids are drawn at 50% probability. Hydrogen atoms and NO_3^- are omitted for clarity. (D) A polymeric chain formed by H–bonding interactions in **C1**.

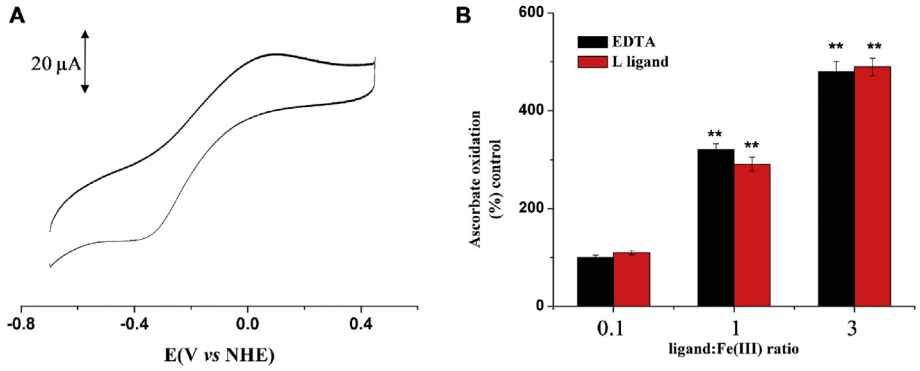

Fig. 2. (A) Cyclic voltammograms of the **C1** prepared in this investigation. Sweep rate, 100 mV/s; solvent MeCN:H_2O (7:3) with 0.1 M Et_4NClO_4. (B) Effect of the Fe(III) complex of the L ligand on ascorbate oxidation. Results are mean ± SD (three experiments, (**) $p < 0.01$).

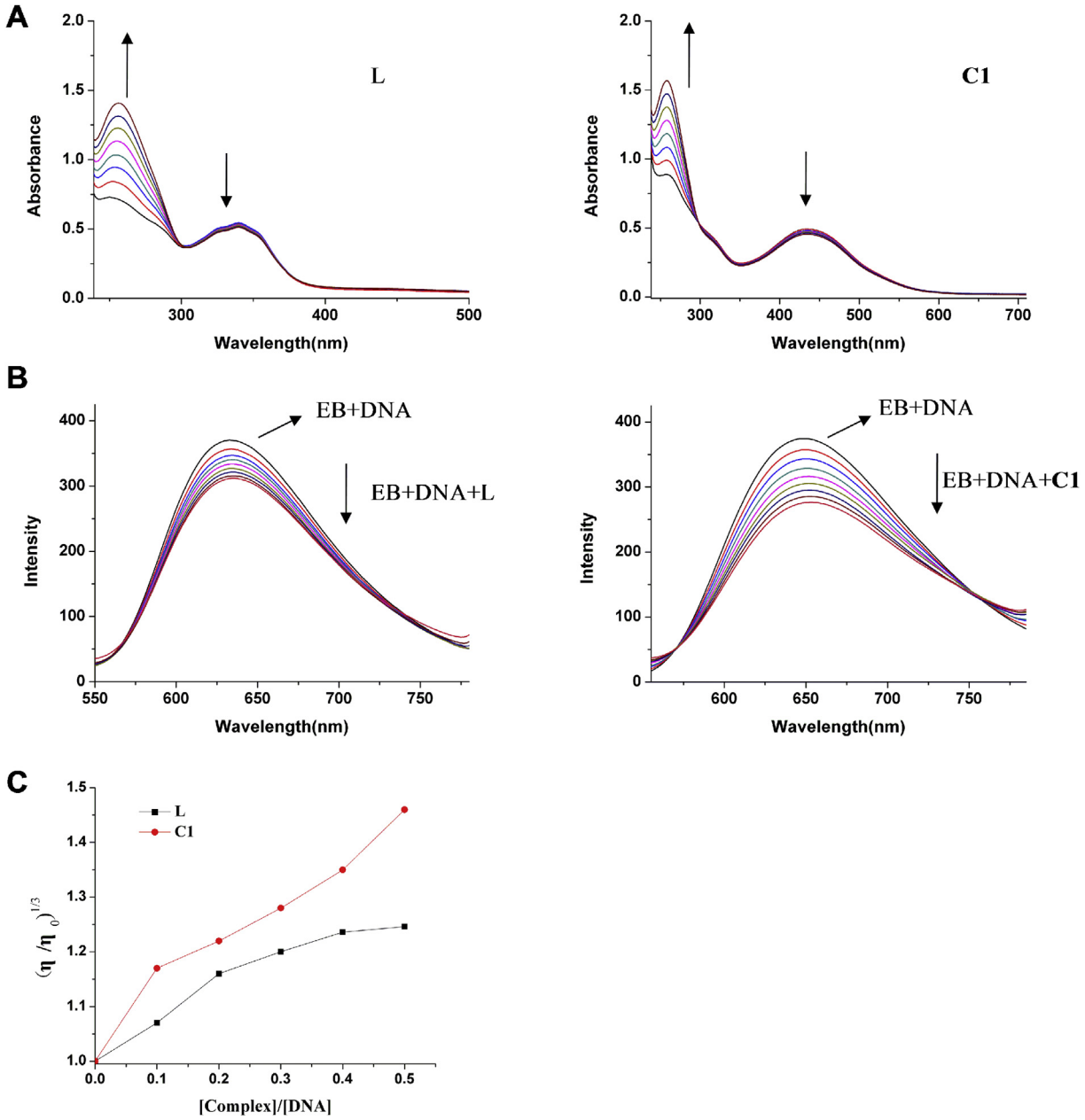

Fig. 3. (A) Absorption spectra of L and complex **C1** (20 μM) upon the titration of CT-DNA (0–70 μM). (B) Fluorescence quenching curves of ethidium bromide bound to DNA: ligand L and the complex **C1**. [DNA] = 5 μM, [EB] = 2.5 μM, and [complex] = 0–40 μM. (C) Relative viscosity increments of CT-DNA (200 μM) solution bound with L and **C1** with increasing the [complex]/[DNA] ratio.

(Fig. 1B) by the weaker N2–H2···S1^{i} (N2···S1^{i} = 2.396 Å and the N2–H2···S1^{i} angle is 164.0°, symmetry code: (i) 1 − *x*, 2 − *y*, − *z*) hydrogen bonds.

Compound **C1** crystallizes in the orthorhombic system with space group *Pbca*. As shown in Fig. 1C, the iron atom was pseudo–octahedrally coordinated by two N2S tridentate L ligand. All Fe–X bond distances are very similar to the related thiosemicarbazone Schiff base–iron complexes [42–44]. Here, the Fe–N(pyridine) distances [Fe1–N1 = 2.062 Å and Fe1–N5 = 2.056 Å] are relatively longer than the Fe–N(azo) distances [Fe1–N2 = 1.918 Å, and Fe1–N6 = 1.913 Å], indicating the different strength of the bond formed by each of the coordinated nitrogen atoms. The difference in Fe–N bond lengths may arise from constraints involved in chelate–ring formation or from the differing positions which N(pyridine) and N(azo) occupy in the coordination polyhedron, as well as from differential Fe→N back donation. The four five–membered chelate rings are planar, and the mean planes through the first and second L ligand atoms are almost perpendicular to each other. In the solid state, **C1** was linked into a one–dimensional polymeric chain by N8–H8A···O3^{i} (N8···O3^{i} = 2.917 Å and the N8–H8A···O3^{i} angle is 172.2°, symmetry code: (i) 0.5 − *x*, −0.5 + *y*, *z*) and weaker N4–H4···O2^{ii} (N4···O2^{ii} = 2.955 Å and the N4–H4···O2^{ii} angle is 164.6°, symmetry code: (ii) −0.5 + *x*, *y*, 1.5 − *z*) hydrogen bonds (Fig. 1D).

L ligand can be represented by two tautomeric forms, the thione form and thiol form (the transfer of the N–N**H**–C proton to the sulfur atom). In the case, the C–S bonds (C7–S1 and C25–S2) of average 1.745 Å in the compound **C1** (thiol form) were longer than this in the L ligand (C7–S1 = 1.672 Å, thione form), indicating that the thiocarbonyl moiety in the compound **C1** adopted a tautomeric form and acted as a mono–negative ligand, which support thiolate formation in the ligands on complexation. To shed light on the energies involved in the process of conformational change of L ligand in methanol, quantum chemical calculations were performed. The calculations show that withdrawal of H from the N–N**H**–C fragment of L and its location on the S atom provokes an energy increase of 13.73 kcal/mol. This is in agreement with previously obtained result on similar systems [45]. The result implies that in solution the L ligand exists almost exclusively in the thione form and that forming the HS–C tautomer prior to complexation is necessary.

3.2. Cyclic voltammetry

The redox activity has been linked with cytotoxicity of complexes of the thiosemicarbazones, particularly their Fe complexes [31,46]. By use of cyclic voltammetry, the $Fe^{II/III}$ redox potentials were determined in a mixture of H_2O and MeCN (3:7 v/v) to ensure sufficient solubility. From inspection of Fig. 2A, the electrochemistry is complicated, and the voltametric waves are only quasi–reversible. In relation to biological activity, the measured $Fe^{II/III}$ redox potentials of $[Fe(L)_2]^+$, like that of other similar thiosemicarbazones Fe complexes such as $[Fe(DpT)_2]^+$, which lie within the range accessible to both cellular oxidants and reductants, and both the ferric and the ferrous forms are chemically stable [30]. Thus, **C1** could redox cycle to generate intracellular ROS.

3.3. Ascorbate oxidation studies

The cyclic voltammetry experiments reported above suggest that the **C1** complex can undergo facile interconversion between the ferrous and ferric states. Hence, it was important to confirm the ability of the **C1** complex to mediate the oxidation of a physiological substrate. Thus, the oxidation of ascorbate catalyzed by the **C1** complex was assessed, and EDTA was also included to act as positive control [38]. In the study, a range of iron–binding equivalents ratios (the L ligand is tridentate chelators and form 1:2 iron/ligand complex, while EDTA is hexadentate and forms 1:1 iron/ligand complex) were examined, namely 0.1, 1, and 3. As shown in Fig. 2B, the iron EDTA complex demonstrated the greatest activity at increasing ascorbate oxidation. For **C1** complex, a marked increase in ascorbate oxidation was found upon increasing the iron–binding equivalents ratios from 0.1 to 1 and 3. This result is also in agreement with the cyclic voltammetry data presented, which demonstrated that the **C1** complex, similar other thiosemicarbazones Fe complexes [38,47], shows considerable redox activity.

3.4. DNA binding properties

DNA is the primary intracellular target of antitumor drugs, thus the interaction between DNA and metallodrug is of paramount importance in understanding the mechanism. In order to have an insight on the binding propensity and binding mode, the mode and propensity for binding of free ligand and complex **C1** to calf-thymus DNA (CT-DNA) were studied with multiple techniques such as absorption and emission spectral studies. Upon addition of DNA to the solution of L, the absorption bands at 340 nm exhibited a hypochromism of about 6.1% without any shift in the wavelength of absorption (Fig. 3A). However, complex **C1** exhibited a hypochromism of about 11.6% with a hypsochromic shift of 1 nm at 446 nm (Fig. 3A), which indicated that the complex was bound to CT-DNA via an intercalative mode. In order to affirm quantitatively the affinity of the complexes bound to DNA, the intrinsic binding constants (K_b) of the compounds with DNA was obtained by using eqn. (1). The K_b values were found to be 0.83×10^4 M^{-1} for L and 1.16×10^4 M^{-1} for **C1**. The observed values of K_b revealed that the ligand and the **C1** complex bind to DNA via intercalative mode [48].

To further investigate the interaction mode between the Fe complex and DNA, we carried out EB fluorescence displacement experiments. As shown in Fig. 3A, **C1** has UV absorption at excitation wavelength (530 nm) and thus some inner-filter effect is present, which results in a decrease in the observed fluorescence intensity. This effect can be approximately corrected with the

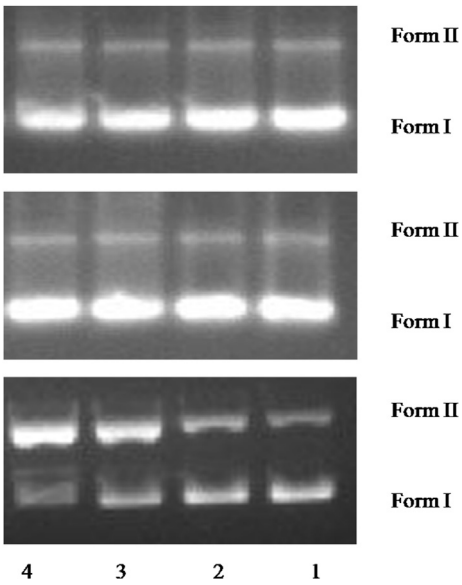

Fig. 4. Agarose gel electrophoresis patterns for the cleavage of pBR322 DNA by complex $Fe(NO_3)_3$, L and **C1** (from top to bottom) at pH 7.0 at 37 °C. Lane 1: DNA alone; Lanes 2–4: DNA with complexes at the concentrations of 10, 15, 20 μM, respectively.

convenient formula $F_{corr} = F_{obs} \times 10^{A(\lambda ex)/2} \times 10^{A(\lambda em)/2}$ (where F_{corr} is the correct fluorescence, F_{obs} the measured fluorescence intensity, and $A(\lambda ex)$ and $A(\lambda em)$ the values of absorbance at the emission and excitation wavelength, respectively) [49,50]. The emission spectra of the EB–DNA system in the absence and presence of L and **C1** (corrected) are shown in Fig. 3B. The addition of the complexes results in a decrease of the fluorescence intensity of the emission band of the DNA-EB system indicate that the complexes would efficiently compete with EB for intercalative binding sites on DNA by replacing EB. According to eqn. (2), K_{app} values are evaluated as 1.31×10^5 M^{-1} and 3.67×10^5 M^{-1} for L and complex **C1**, respectively. The higher values of K_{app} for complex **C1** indicated the stronger binding ability toward DNA than free ligand L, which is consistent with the electronic absorption spectral results. Moreover, the values of K_{app} were less than the binding constant of the classical intercalators and metallointercalators (10^7 M^{-1}), especially for L, which suggested that the interaction between the planar aromatic L and DNA was a moderate intercalative mode.

To further investigate the binding nature of the complexes with DNA, viscosity measurements on the solutions of DNA incubated with the L and complex **C1** have been carried out. Viscosity measurement is regarded as the most critical method to detect the binding mode between DNA and small agents, which can monitor the DNA length changes, classical intercalation leads to an

Table 3
IC_{50}^{a} (μM) of HL and **C1** for the selected cells for 48 h.

Compound	Cell growth inhibition, IC_{50} ± SD (μM)					
	HepG2	HeLa	HL-7702	MCF-7	MCF-7/ADR	RF[b]
HL	>40	>40	>40	>40	>40	
C1	0.23 ± 0.02	0.46 ± 0.02	1.62 ± 0.12	1.1 ± 0.07	1.38 ± 0.05	1.2
*Cis*platin	22.47 ± 1.72	27.57 ± 1.81	10.39 ± 1.23	20.7 ± 1.91	21.39 ± 1.68	1.1
Doxorubicin				2.78 ± 0.17	>40	>14

[a]IC_{50} values are presented as the mean ± SD from three separated experiments. RF^{b} = IC_{50} (MCF-7)/IC_{50} (MCF-7/ADR).

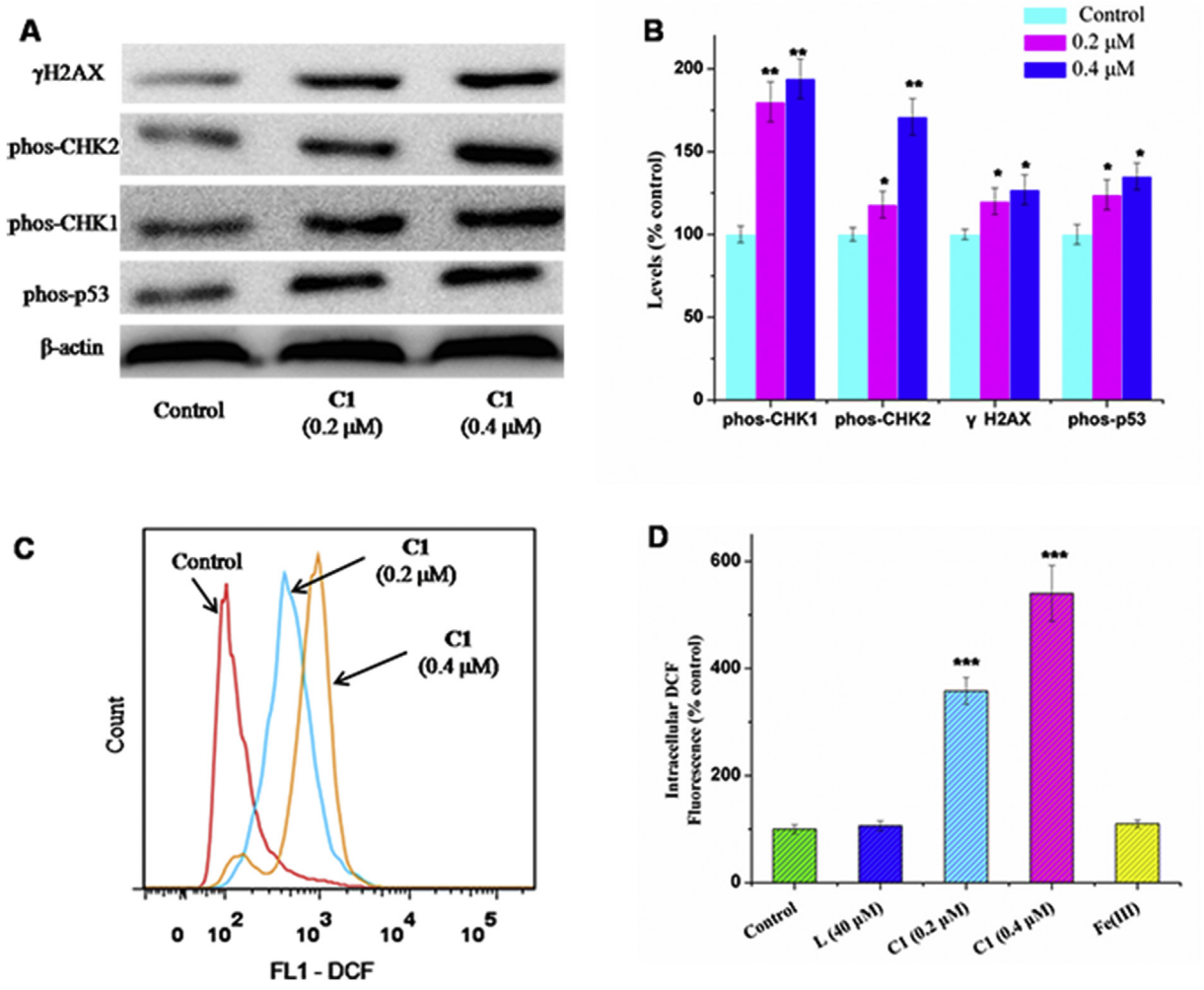

Fig. 5. (A) Immunoblotting analysis of proteins (γH2AX, phos–CHK1, phos–CHK2 and phos–p53) related to the DNA damage pathway. β–Actin was assessed as a loading control. (B) Percentage expression levels of γH2AX, phos–CHK1, phos–CHK2 and phos–p53. The percentage values are those relative to the control. (C) Analysis of ROS levels by flow cytometry after HepG2 cells were treated with vehicle and **C1** at indicated concentrations for 24 h and stained with H_2DCFDA. (D) Quantification of the flow cytometric results in (C) showing the percentage of cells with increased intracellular DCF oxidation compared to control cells. Results are the mean ± SD (n = 3): (*) $p < 0.05$, (**) $p < 0.01$, (***) $p < 0.001$.

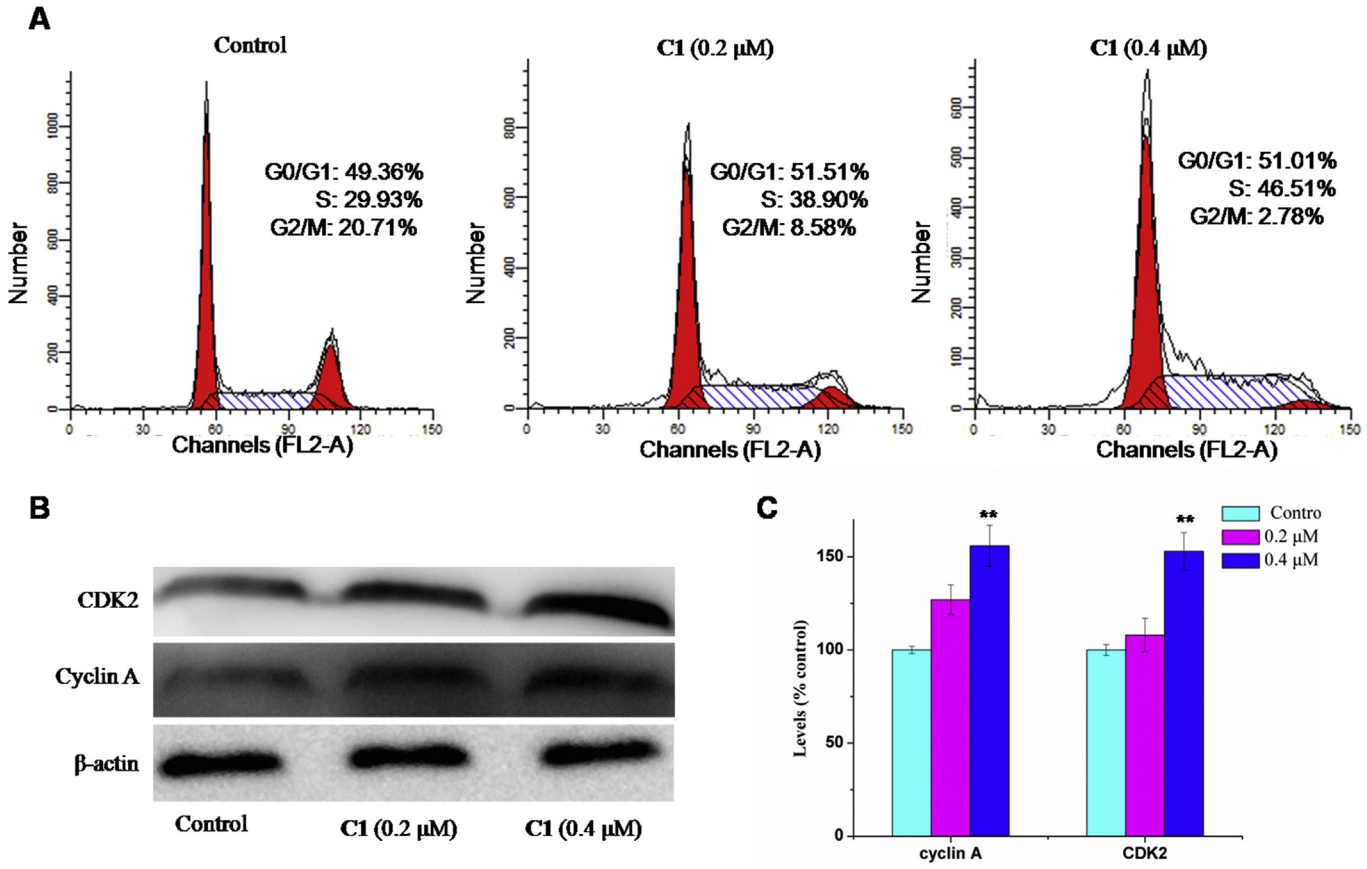

Fig. 6. (A) Cell cycle contributions resulting from treatment with **C1** (0.2 and 0.4 μM) for 24 h. (B) Representative Western blots of the effects of **C1** on the protein expression levels of CDK2 and cyclin A. β–Actin was assessed as a loading control. (C) Percentage expression levels of CDK2 and cyclin A. The percentage values are those relative to the control. Results are the mean ± SD (n = 3): (**) $p < 0.01$.

increased DNA viscosity and groove binding or electrostatic mode results in not apparent alteration in DNA viscosity [51,52]. The relative viscosities of CT-DNA in the presence of the complexes are shown in Fig. 3C. Upon continuous addition of the complexes, the relative viscosity of DNA increases efficiently. The result suggests complex could bind to DNA by intercalation, which rules out the groove binding interactions or electrostatic between DNA and complex [53].

3.5. pBR322 plasmid DNA cleavage activity

Most previously reported metal complexes are capable of catalyzing the cleavage of DNA [54]. We therefore examined whether L and complex **C1** exhibited DNA-cleaving activities using an agarose gel electrophoresis assay. It can be seen from Fig. 4 that complex **C1** could efficiently relax the supercoiled form (Form I) of DNA into an open circular form (Form II) in a concentration-dependent fashion. It should be noted that under the same condition, free ligand L and $Fe(NO_3)_3$ did not exhibit any cleavage activity. Thus, the cleavage properties of the present complexes are attributed to the proximity of the DNA-bound complexes to the deoxyl ribose rings and the coordination geometries of complexes, as understood from the spectral and electrochemical properties [55].

3.6. Cytotoxic activity of the Fe(III) complex

Previous studies have illustrated that complexation of thiosemicarbazones chelators with metal ions can result in marked changes in biological activity [28,31,32]. To determine the effect of complexation on the antiproliferative efficacy of L ligand with Fe(III), we performed MTT assays using various cancer cells and one normal liver cell HL-7702. In comparison with the free ligand, the **C1** demonstrated significantly increased antiproliferative activity after a 48 h incubation, while no pronounced antiproliferative effect was observed with $Fe(NO_3)_3$ alone (Table 3). The result may be that relative to the ligand, the Fe complex is more able to cross the cell membrane because of its predicted greater lipophilicity [31,56]. In addition, in MCF-7/ADR cells, the resistance factor values for the **C1** was roughly 14 times lower than that of Doxorubicin, suggesting that the Fe complex is not potential multidrug-resistant substrates.

3.7. Possible anticancer mechanism of the Fe(III) complex

Most previously reported metal compounds are assumed to induce cell death through DNA damage [57]. Therefore, immunoblotting analyses were conducted to monitor changes in expression of biomarkers related to the DNA damage pathway. HepG2 cells incubated for 48 h with **C1** showed a marked increase in expression of the phosphorylated forms of H2AX (γH2AX), CHK1, CHK2, and p53 (Ser15) proteins (Fig. 5A and B), indicating that **C1** kill cells by damaging DNA [58–60].

Excess intracellular ROS, including H_2O_2, O_2^- and HO^-, could cause DNA damage and trigger p53 activation [61–63]. To confirm the redox activity of **C1** complex as suggested by the electrochemical and ascorbate oxidation studies, the ability of this complex to catalyze the production of intracellular ROS in HepG2 cells was assessed using the fluorescent DCF probe and flow cytometry. Flow cytometry analysis results show that **C1** can significantly

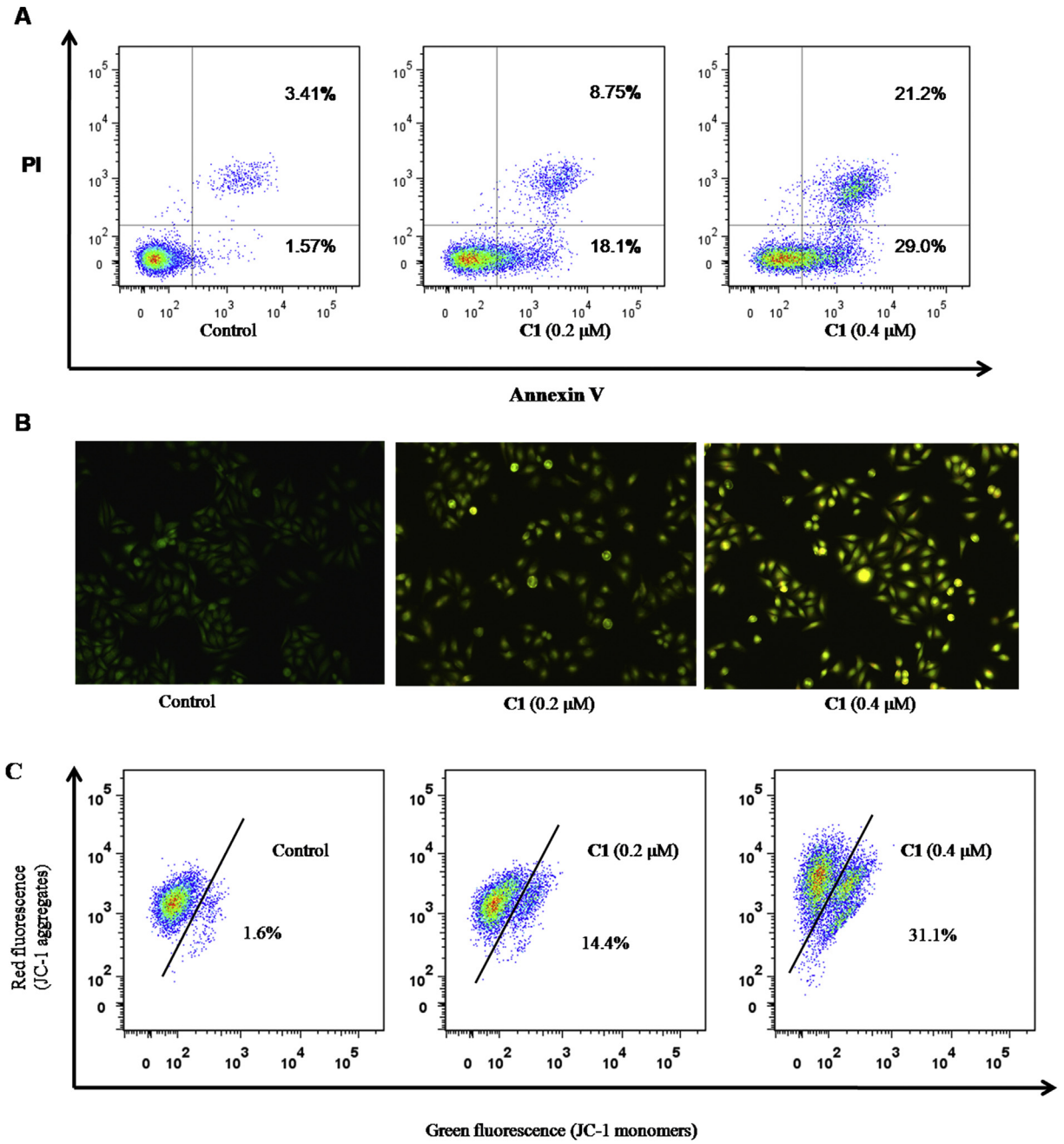

Fig. 7. (A) Representative dot plots of PI and annexinV double staining on the HepG2 cells in the presence of the indicated concentrations of **C1** for 24 h. (B) Representative images of AO/EB double stained HepG2 cells after treatment with **C1** at the indicated concentrations for 24 h. (C) Effects of **C1** on mitochondrial membrane potential analyzed by JC−1 staining and flow cytometry. HepG2 cells were treated with vehicle, and **C1** at the indicated concentrations indicated for 24 h.

increase the intracellular ROS levels (Fig. 3C). The DCF fluorescence peaks for each concentration evaluated were quantified. These data reveal a significant ($p < 0.001$) increase in H_2DCF oxidation to 358± 12% and 540± 15% of control cells at 0.2 and 0.4 μM, respectively (Fig. 5D). However, no significant increase in H_2DCF oxidation was observed with the same concentrations of L ligand and Fe(III) alone over this same incubation period. These results suggest that **C1** complex' marked antitumor activity may due to their ability to generate cytotoxic ROS during a redox cycle [64]. In addition, cancer cells exhibit greater ROS stress than normal cells [65]. Therefore, elevation of the ROS levels by metal−drugs may be a way to selectively kill cancer cells without causing significant damage to normal cells.

Cell cycle arrest and apoptosis are two of the most common cellular response to DNA damage [66,67]. Therefore, flow cytometric analysis was carried out to examine the effects of **C1** on HepG2 cell cycle distribution. As depicted in Fig. 6A, comparison with untreated control, the percentage of G2/M−phase decreases to 8.58± 1.5% and 2.78± 2.3% 13.2 at **C1** concentrations of 0.2 and 0.4 μM, respectively. The percentages of cells in the S phase increased to 38.90± 3.3% and 46.20± 2.1%, at the same **C1** concentrations. These results indicated that **C1** induced a dose-dependent S−phase arrest of HepG2 cells. Progression through the cell cycle is tightly controlled by cyclins complexes and cyclin−dependent kinases (CDKs) at different phases [68]. To explore the molecular mechanisms of **C1**-induced S−phase block,

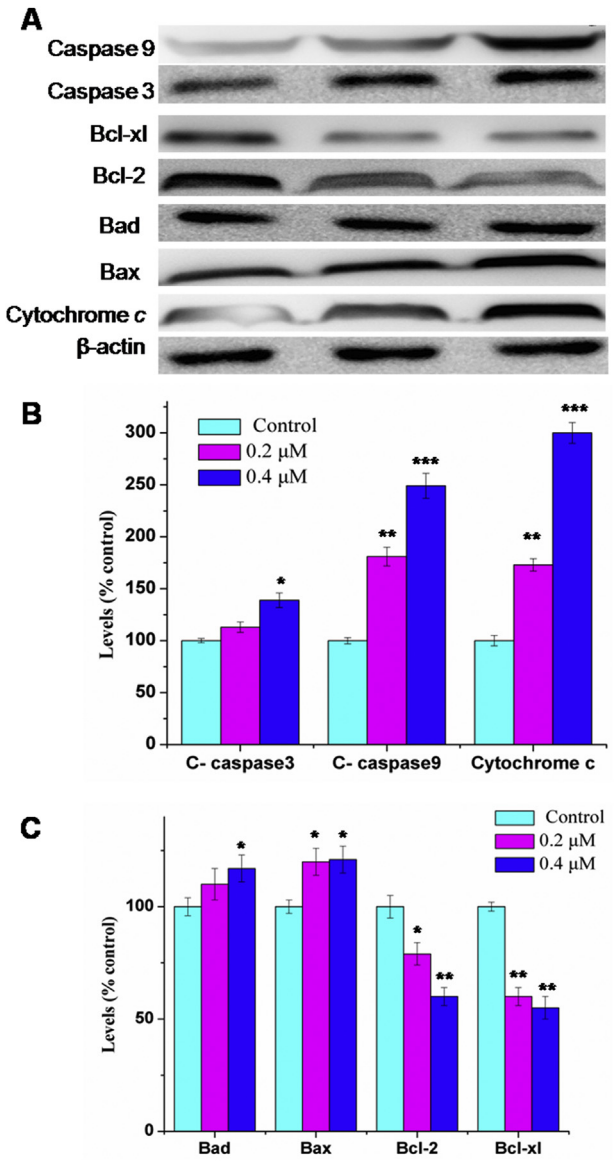

Fig. 8. (A) Western blot analysis of cleaved Caspase−3, cleaved Caspase−9, Bcl−2, Bcl−xl, Bad, Bax and cytochrome *c* in HepG2 cells treated with different concentrations of **C1** for 48 h. (B) Percentage expression levels of Bcl−2, Bcl−xl, Bad, and Bax. (C) Percentage expression levels of cleaved Caspase−3, cleaved Caspase−9 and Cytochrome *c*. The percentage values are those relative to the control. Results are the mean ± SD (n = 3): (*) $p < 0.05$, (**) $p < 0.01$, (***) $p < 0.001$.

the expression of S phase−specific cell cycle regulatory proteins (major CDK2 and cyclin A) were examined by immunoblotting analyses. Compared with the vehicle−treated control, CDK2 and cyclin A increased significantly upon **C1** treatment (Fig. 6B and C), suggesting that activation of cyclin A/CDK2 might play a important role in **C1**−mediated growth S−phase arrest.

Many metal cancer drugs exert their cytotoxic effects through apoptosis, and we therefore monitored features related to this pathway [69–71]. Using a dual Annexin V staining/PI flow cytometry assay, we explored the occurrence of apoptosis in HepG2 cells treated for 24 h with **C1**. As can be seen from Fig. 7A, **C1** can efficiently induce apoptosis in HepG2 cells. Even at a low concentration of 0.2 μM, **C1** prompts a large population of cells to undergo early (18.1%) and late (8.75%) stage apoptosis. To gain more evidence for the apoptotic cell death induced by **C1** complex, the apoptosis−inducing properties such as cytoplasmic shrinkage, chromatin condensation, or apoptotic−body formation were further examined by AO/EB staining. As shown in Fig. 7B, HepG2 cells treated with **C1** display a dose−dependent morphological change. These results provide validation for the apoptosis pathway.

Mitochondrial dysfunction plays an important role in triggering apoptosis, which is demonstrated by several key events such as the reduction of mitochondrial membrane potential ($\Delta\psi_m$), the onset of mitochondrial permeability transition, and the release of cytochrome *c* [72]. To establish whether apoptosis induced by **C1** is related to mitochondrial dysfunction, $\Delta\psi_m$ was evaluated by flow cytometry using JC−1 staining. Treatment of HepG2 cells with **C1** cause a decrease the $\Delta\psi_m$ level in a concentration−dependent manner (Fig. 7C), which confirmed the activation of mitochondria mediated apoptosis. The Bcl-2 family proteins have been described as key regulators of $\Delta\psi_m$ [73]. Previously, many studies have demonstrated that metal complexes induced mitochondria mediated apoptosis in cancer cells through regulation of Bcl-2 family members [74–77]. In the present study, Western blot analysis revealed that **C1** upregulated the expression of Bax and Bad (proapoptosis Bcl-2 family proteins), and suppressed the expression of Bcl-xl and Bcl-2 (prosurvival Bcl-2 family proteins) (Fig. 8A–C). The ratio of Bcl-xl/Bad and Bcl-2/Bax is decreased, leading to the release of apoptogenic factors, such as cytochrome *c*. Subsequently, cytochrome *c* caused activation of caspase-3, and -9. These results indicate that **C1** can induce mitochondria mediated apoptosis in HepG2 cells through regulating the expression of Bcl-2 family proteins.

4. Conclusion

In this study, we synthesized an α−*N*−heterocyclic thiosemicarbazone Fe(III) complex, and investigated its anticancer activity and explored the underlying molecular mechanisms. DNA binding and cleavage experiments indicated that the Fe(III) complex exhibited the high pBR322 DNA cleaving ability and the high binding affinity toward CT-DNA. The Fe complex−induced DNA damage and ROS overproduction induces phosphorylation of p53 and upregulate the expression of cyclin A/CDK2, leading to S phase arrest. On the one hand, the activation of p53 induces the mitochondrial dysfunction through regulating the expression of Bcl−2 family proteins, and then triggered the mitochondrial release of apoptogenic factors, like cytochrome *c* and caused cleavage of caspase family proteases such as caspase-3 and -9, finally resulting in apoptosis. On the basis of these results, we suggest that the thiosemicarbazone Fe complex with multi−death pathways may be a candidate for further evaluation as a chemopreventive and chemotherapeutic agent for human cancers.

Acknowledgements

This work was supported by the Natural Science Foundation of China (31460232), Natural Science Foundation of Guangxi (2014GXNSFDA118016), Ministry of Education of China (CMEMR2015-A01).

Appendix A. Supplementary data

Supplementary data related to this article can be found at http://dx.doi.org/10.1016/j.ejmech.2016.07.041.

References

[1] K.D. Mjos, C. Orvig, Chem. Rev. 114 (2014) 4540–4563.
[2] L. Kelland, Nat. Rev. Cancer 7 (2007) 573–584.
[3] G. Gasser, I. Ott, N. Metzler−Nolte, J. Med. Chem. 54 (2011) 3–25.

[4] M.A. Jakupec, M. Galanski, V.B. Arion, C.G. Hartinger, B.K. Keppler, Dalton Trans. 2 (2008) 183–194.
[5] P.J. Dyson, G. Sava, Dalton Trans. (2006) 1929–1933.
[6] S.M. Schmitt, M. Frezza, Q.P. Dou, Front. Biosci. Sch. Ed. 4 (2012) 375–391.
[7] J.M. Pérez, M.A. Fuertes, C. Alonso, C. Navarro-Ranninger, Crit. Rev. Oncol. Hematol. 35 (2000) 109–120.
[8] C.X. Zhang, S.J. Lippard, Curr. Opin. Chem. Biol. 7 (2003) 481–489.
[9] N.C.N. Andrews, Engl. J. Med. 341 (1999) 1986–1995.
[10] T.C. Iancu, H. Shiloh, A. Kedar, Cancer 61 (1988) 2497–2502.
[11] N.T. Le, D.R. Richardson, Biochim. Biophys. Acta 1603 (2002) 31–46.
[12] D.R. Richardson, E. Baker, Biophys. Acta 1053 (1990) 1–12.
[13] E.H. Morgan, Mol. Asp. Med. (1981) 1–123.
[14] J.W. Larrick, P. Cresswell, J. Supramol. Struct. 11 (1979) 579–586.
[15] H.L. Elford, M. Freese, E. Passamani, H.P. Morris, J. Biol. Chem. 245 (1970) 5228–5233.
[16] L. Thelander, P. Reichard, Annu. Rev. Biochem. 48 (1979) 133–158.
[17] G.Y. Lui, Z. Kovacevic, V. Richardson, A.M. Merlot, D.S. Kalinowski, D.R. Richardson, Oncotarget 6 (2015) 18748–18779.
[18] E. Gumienna–Kontecka, M. Pyrkosz–Bulska, A. Szebesczyk, M. Ostrowska, Curr. Med. Chem. 21 (2014) 3741–3767.
[19] D.J. Lane, T.M. Mills, N.H. Shafie, A.M. Merlot, R. Saleh Moussa, D.S. Kalinowski, Z. Kovacevic, D.R. Richardson, Biochim. Biophys. Acta 1845 (2014) 166–181.
[20] D.R. Richardson, P.C. Sharpe, D.B. Lovejoy, D. Senaratne, D.S. Kalinowski, M. Islam, P.V. Bernhardt, J. Med. Chem. 49 (2006) 6510–6521.
[21] Y. Yu, D.S. Kalinowski, Z. Kovacevic, A.R. Siafakas, P.J. Jansson, C. Stefani, D.B. Lovejoy, P.C. Sharpe, P.V. Bernhardt, D.R. Richardson, J. Med. Chem. 52 (2009) 5271–5294.
[22] D.S. Kalinowski, D.R. Richardson, Pharmacol. Rev. 57 (2005) 547–583.
[23] H. Huang, Q. Chen, X. Ku, L. Meng, L. Lin, X. Wang, C. Zhu, Y. Wang, Z. Chen, M. Li, H. Jiang, K. Chen, J. Ding, H. Liu, J. Med. Chem. 53 (2010) 3048–3064.
[24] É.A. Enyedy, M.F. Primik, C.R. Kowol, V.B. Arion, T. Kiss, B.K. Keppler, Dalton Trans. 40 (2011) 5895–5905.
[25] R.W. Brockman, J.R. Thomson, M.J. Bell, H.E. Skipper, Cancer Res. 16 (1956) 167–170.
[26] C.M. Nutting, C.M.L. van Herpen, A.B. Miah, S.A. Bhide, J.P. Machiels, J. Buter, C. Kelly, D. de Raucourt, K.J. Harrington, Ann. Oncol. 20 (2009) 1275–1279.
[27] J.F. Zeidner, J.E. Karp, A.L. Blackford, B.D. Smith, I. Gojo, S.D. Gore, M.J. Levis, H.E. Carraway, J.M. Greer, S.P. Ivy, K.W. Pratz, M.A. McDevitt, Haematologica 99 (2014) 672–678.
[28] P.J. Jansson, P.C. Sharpe, P.V. Bernhardt, Des R. Richardson, J. Med. Chem. 53 (2010) 5759–5769.
[29] J. Yuan, D.B. Lovejoy, D.R. Richardson, Blood 104 (2004) 1450–1458.
[30] P.V. Bernhardt, P.C. Sharpe, M. Islam, D.B. Lovejoy, D.S. Kalinowski, Des R. Richardson, J. Med. Chem. 52 (2009) 407–415.
[31] D.S. Kalinowski, Y. Yu, P.C. Sharpe, M. Islam, Y.T. Liao, D.B. Lovejoy, N. Kumar, P.V. Bernhardt, D.R. Richardson, J. Med. Chem. 50 (2007) 3716–3729.
[32] P.V. Bernhardt, P.C. Sharpe, M. Islam, D.B. Lovejoy, D.S. Kalinowski, D.R. Richardson, J. Med. Chem. 52 (2009) 407–415.
[33] G.M. Sheldrick, SHELXTLV5.1, Software, Reference, Manual, BrukerAXS, Inc, Madison, W.I. U.S.A, 1997.
[34] M.W. Schmidt, K.K. Baldridge, J.A. Boatz, S.T. Elbert, M.S. Gordon, J.H. Jensen, S. Koseki, N. Matsunaga, K.A. Nguyen, S.J. Su, T.L. Windus, M. Dupuis, J. Montgomery, J. Comput. Chem. 14 (1993) 1347–1363.
[35] A.D. Becke, J. Chem. Phys. 98 (1993) 5648–5652.
[36] C. Lee, W. Yang, R.G. Parr, Phys. Rev. B37 (1988) 785–789.
[37] J. Tomasi, B. Mennucci, E. Cances, Theochem 464 (1999) 211–226.
[38] C. Stefani, P.J. Jansson, E. Gutierrez, P.V. Bernhardt, D.R. Richardson, D.S. Kalinowski, J. Med. Chem. 56 (2013) 357–370.
[39] T.B. Chaston, D.R. Richardson, J. Biol. Inorg. Chem. 8 (2003) 427–438.
[40] M. Alagesan, N.S.P. Bhuvanesh, N. Dharmaraj, Dalton Trans. 42 (2013) 7210–7223.
[41] M. Lee, A.L. Rhodes, M.D. Wyatt, S. Forrow, J.A. Hartley, Biochemistry 32 (1993) 4237–4245.
[42] E.W. Yemeli, G.R. Blake, A.P. Douvalis, T. Bakas, G.O. Alberda van Ekenstein, P.J. van Koningsbruggen, Chem. Eur. J. (2010), http://dx.doi.org/10.1002/chem.201002100.
[43] V. Amendola, M. Boiocchi, L. Fabbrizzi, L. Mosca, Chem. Eur. J. 14 (2008) 9683–9696.
[44] M. Li, J. Zhou, H. Zhao, C. Chen, J. Wang, J. Coord. Chem. 62 (2009) 1423–1429.
[45] M. Krasowska, A. Kochel, A. Filarowski, CrystEngComm 12 (2010) 1955–1962.
[46] D.R. Richardson, D.S. Kalinowski, V. Richardson, P.C. Sharpe, D.B. Lovejoy, M. Islam, P.V. Bernhardt, J. Med. Chem. 52 (2009) 1459–1470.
[47] C. Stefani, G. Punnia-Moorthy, D.B. Lovejoy, P.J. Jansson, D.S. Kalinowski, P.C. Sharpe, P.V. Bernhardt, D.R. Richardson, J. Med. Chem. 54 (2011) 6936–6948.
[48] J. Olmsted, D.R. Kearns, Biochemistry 16 (1977) 3647–3654.
[49] L. Stella, A.L. Capodilupo, M. Bietti, Chem. Commun. (2008) 4744–4746.
[50] M. van de Weert, L. Stella, J. Mol. Struct. 998 (2011) 144–150.
[51] B.L. Fei, Z.X. Huang, W.S. Xu, D.D. Li, Y. Lu, W.L. Gao, Y. Zhao, Y. Zhang, Q.B. Liu, J. Photochem. Photobiol. B160 (2016) 43–52.
[52] Y. Zhang, J.Y. Wen, M.H. Mahmood, X.L. Wang, B.B. Lv, X. Ying, H. Wang, L.N. Ji, H.Y. Liu, Luminescence 30 (2015) 1045–1054.
[53] J.L. Li, L. Jiang, B.W. Wang, J.L. Tian, W. Gu, X. Liu, S.P. Yan, J. Inorg. Biochem. 145 (2015) 19–29.
[54] M. Chen, X.Y. Tang, S.P. Yang, H.H. Li, H.Q. Zhao, Z.H. Jiang, J.X. Chen, W.H. Chen, Dalton Trans. 44 (2015) 13369–13377.
[55] M. Alagesan, N.S.P. Bhuvanesh, N. Dharmaraj, Eur. J. Med. Chem. 78 (2014) 281–293.
[56] P.V. Bernhardt, J. Mattsson, D.R. Richardson, Inorg. Chem. 45 (2006) 752–760.
[57] K. Suntharalingam, T.C. Johnstone, P.M. Bruno, W. Lin, M.T. Hemann, S.J. Lippard, J. Am. Chem. Soc. 135 (2013) 14060–14063.
[58] S. Matsuoka, G. Rotman, A. Ogawa, Y. Shiloh, K. Tamai, S.J. Elledge, Proc. Natl. Acad. Sci. U.S.A. 97 (2000) 10389–10394.
[59] J.Y. Ahn, J.K. Schwarz, H. Piwnica–Worms, C.E. Canman, Cancer Res. 60 (2000) 5934–5936.
[60] S.Y. Shieh, M. Ikeda, Y. Taya, C. Prives, Cell 91 (1997) 325–334.
[61] I.R. Indran, M.P. Hande, S. Pervaiz, Cancer Res. 71 (2011) 266–276.
[62] K.–R. Park, D. Nam, H.–M. Yun, S.–G. Lee, H.–J. Jang, G. Sethi, S.K. Cho, K.S. Ahn, Cancer Lett. 312 (2011) 178–188.
[63] Z. Luo, L. Yu, F. Yang, Z. Zhao, B. Yu, H. Lai, K.H. Wong, S.M. Ngai, W. Zheng, T. Chen, Metallomics 6 (2014) 1480–1490.
[64] D.B. Lovejoy, P.J. Jansson, U.T. Brunk, J. Wong, P. Ponka, D.R. Richardson, Cancer Res. 71 (2011) 5871–5880.
[65] D. Trachootham, J. Alexandre, P. Huang, Nat. Rev. Drug. Discov. 8 (2009) 579–591.
[66] H. Lai, Z. Zhao, L. Li, W. Zheng, T. Chen, Metallomics 7 (2015) 439–447.
[67] R. Sinha, K. Ei-Bayoumy, Curr. Cancer Drug Targets 4 (2004) 13–28.
[68] J. Bloom, F.R. Cross, Nat. Rev. Mol. Cell Biol. 8 (2007) 149–160.
[69] E.R. Jamieson, S.J. Lippard, Chem. Rev. 99 (1999) 2467–2498.
[70] D. Wang, S.J. Lippard, Nat. Rev. Drug Discov. 4 (2005) 307–320.
[71] U. Fischer, K. Schulze-Osthoff, Cell Death Differ. 12 (Suppl. 1) (2005) 942–961.
[72] C. Wang, R.J. Youle, Annu. Rev. Genet. 43 (2009) 95–118.
[73] S. Cory, J.M. Adams, Nat. Rev. Cancer 2 (2002) 647–656.
[74] N. Wang, Y. Feng, L. Zeng, Z. Zhao, T. Chen, ACS Appl. Mater. Interfaces 7 (2015) 14933–14945.
[75] T. Chen, Y. Liu, W.J. Zheng, J. Liu, Y.S. Wong, Inorg. Chem. 49 (2010) 6366–6368.
[76] Z. Deng, L. Yu, W. Cao, W. Zheng, T. Chen, Chem. Commun. 51 (2015) 2637–2640.
[77] J. Qi, S. Liang, Y. Gou, Z. Zhang, Z. Zhou, F. Yang, H. Liang, Eur. J. Med. Chem. 96 (2015) 360–368.